Journal of Asian Earth Sciences: X 10 (2023) 100168

Contents lists available at ScienceDirect

Journal of Asian Earth Sciences: X

journal homepage: www.sciencedirect.com/journal/journal-of-asian-earth-sciences-x

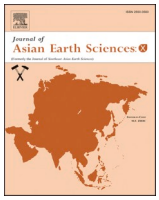

Landslide ground model development through integrated geoelectrical and seismic imaging in Thungsong district, Nakhon Si Thammarat, Thailand

C Sujitapan [a,*], J.M. Kendall [b], J.E. Chambers [c], S Yordkayhun [d]

[a] School of Sciences, Walailak University, Thaiburi, Thasala District, Nakhon Si Thammarat 80161, Thailand
[b] University of Oxford, Department of Earth Sciences, Oxford OX1 3AN, United Kingdom
[c] British Geological Survey, Keyworth, Nottingham NG12 5GG, United Kingdom
[d] Geophysics Research Centre, Department of Physics, Faculty of Science, Prince of Songkla University, Hat Yai, Songkhla 90112, Thailand

ARTICLE INFO

Keywords:
Slope failure
Landslide structure
Electrical resistivity tomography
Seismic refraction tomography
Conceptual ground model

ABSTRACT

A ground model of a shallow landslide in rainfall-induced slope failure of Thungsong, Nakhon Si Thammarat, southern Thailand is developed through an integrated geophysical approach, utilising electrical resistivity tomography and P-wave seismic refraction tomography (SRT) methods. Those two methods were applied to assess landslide structure and study deformation mechanisms along four profiles. Beside the four profiles there is another profile, which was acquired near an borehole and used for the calibration with geological data. Our results show subsurface structures in terms of the ground model used to determine stratigraphic layers, zones of saturation or groundwater table, and significant differences between the landslide slip material and the underlying bedrock. The clay-rich zones (resistivity less than 500 Ωm) in the colluvium on the relatively steep slope, show enhanced potential for landslides. This silty clay plays an important role for landslide activation in this site. Moreover, a combination of steep slopes, shallow basement rocks overlain by clay-rich colluvium, and seasonally high rain fall leads to landslides in the region. The ground model produced by geophysical imaging for this region achieves a comprehensive understanding of the structure and lithology of a complex landslide system and overcomes the limitations of remote-sensing data or isolated intrusive sampling techniques alone.

1. Introduction

Landslides are considered as one of the most destructive natural hazards (Ma et al., 2021). They are not only prevalent in regions with growing population and increasing land use (Reichenbach et al., 2014; Dijkstra et al., 2014; Glendinning et al., 2014), but also aggravated by the global changing climate associated with escalation in extreme weather (Gariano and Guzzetti, 2016; Morelli et al., 2019). Landslides are complex and diverse (McCann and Forster, 1990; Colangelo et al., 2006; Gunn et al., 2013; Merritt et al., 2013). The lithological components and internal structures of individual landscapes are of critical importance in better understanding their driving mechanisms and possible relationships between different landscapes. This can be achieved by using a ground model (Merritt et al., 2013). The ground models of landslide are commonly developed through remote-sensing approaches (de Bari et al., 2011; Confuorto et al., 2017), geotechnical techniques, and geophysical investigations (Merritt et al., 2013). Geotechnical techniques, such as boreholes, cone penetration tests, trenching, and laboratory studies (Fell et al., 2000; Thakur et al., 2023), typically yield results of high resolution, but implementing drilling on steep and unstable slope is expensive, difficult, and labour intensive (Jongmans and Garambois, 2007; Merritt et al., 2013).Instead, geophysical approaches, such as electrical resistivity tomography (ERT) and seismic refraction tomography (SRT), are well-suited to the study of landslide processes, because they provide spatial or volumetric information on the internal structure and physical properties of the subsurface (Yilmaz, 2007; Chambers et al., 2011; Perrone et al., 2014; Whiteley et al., 2019). Moreover, the cost of survey is relatively cheap compared to geotechnical methods and the data acquisition is relatively quick (Jongmans and Garambois, 2007).

In previous studies, the SRT method is mainly applied in landslide investigations to characterise the internal structure, such as geometry, depth of shear zone and bedrock, and thickness of unstable material (Solberg et al., 2016; Whiteley et al., 2019, Imani et al., 2021). This can be used to study the mechanical properties of soils or rocks that make up the landslide (Capizzi and Martorana, 2014). While, the ERT method is

* Corresponding author.
E-mail address: chedtaporn.su@wu.ac.th (C. Sujitapan).

https://doi.org/10.1016/j.jaesx.2023.100168
Received 7 May 2023; Received in revised form 17 November 2023; Accepted 26 November 2023
Available online 29 November 2023

suitable to study landslide structures, through composition in the subsurface (Asriza et al., 2017; Rezaei et al., 2019), and to detect the lateral extent and thickness of landslide materials and the internal geological structure of slopes (Chambers et al., 2011; Falae et al., 2019; Samodra et al., 2020). In addition, the ERT method has been successful to study groundwater and soil moisture variations in unstable slopes (Gance et al., 2014). Consequently, the integration of the P-wave SRT and ERT results through a 2D ground model is powerful for landslide assessment. However, the SRT and ERT methods in previous studies are most effective when they are applied in conjunction with sufficient geotechnical data, such as soil logging from borehole (Chen et al., 2019; Zakaria et al., 2021). Here, the integration of the P-wave SRT and ERT with only one borehole is used to study landslides in Thungsong district, Nakhon Si Thammarat province, southern Thailand (Fig. 1). This study area often experiences landslides due to the combination of mountainous and hilly topography and prolonged seasons of precipitation.

The aim of this study is to produce a comprehensive ground model to characterize internal slope structure and to study landslide deformation mechanisms in Thungsong landslide, where is a remote and difficult accessible area. The primary purpose of this ground model is to provide

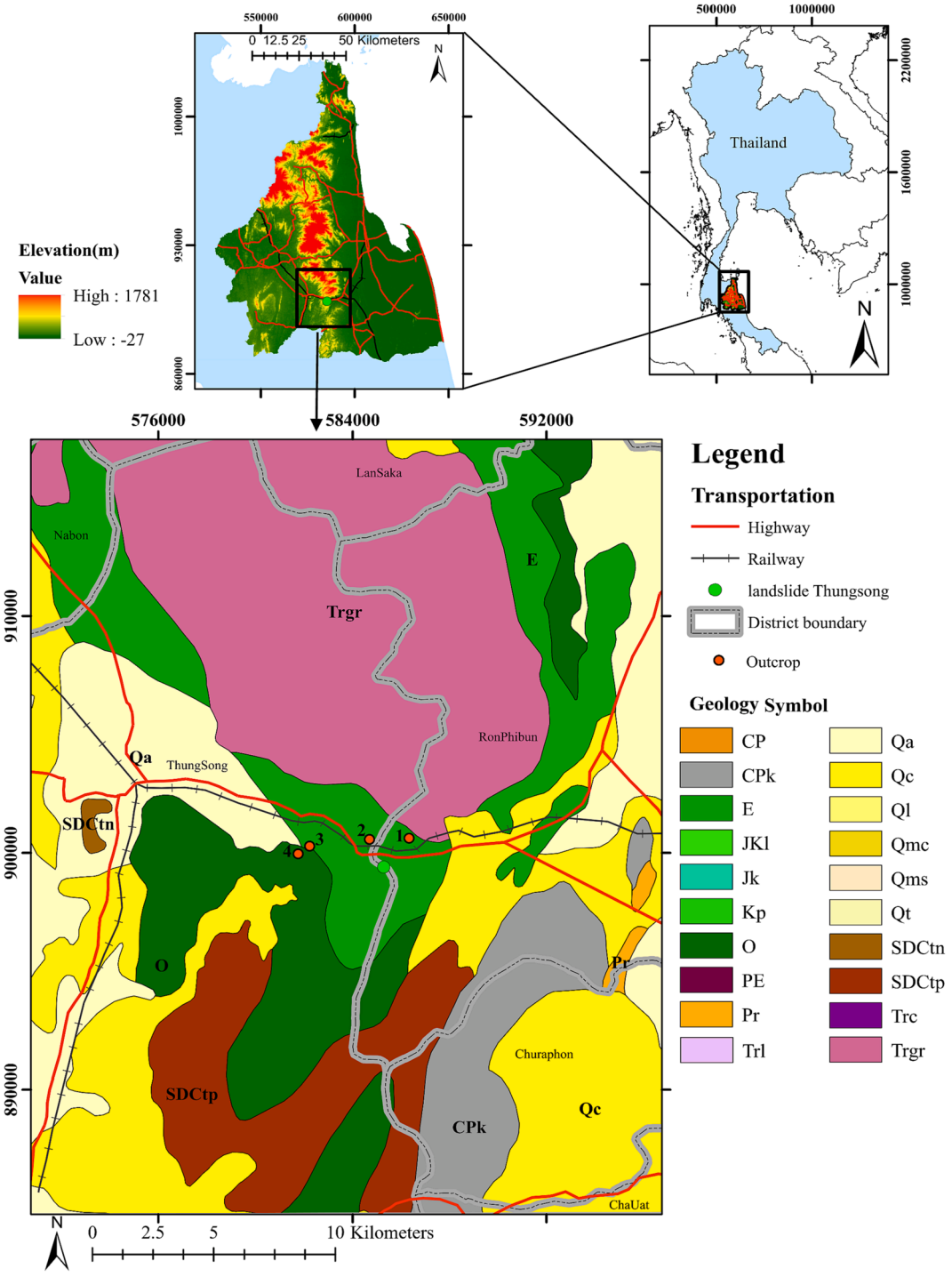

Fig. 1. Geological map of study area and 30 m-DEM of Nakhon Si Thammarat province, showing the position of fieldwork (light green circle), positions of outcrops (orange circles). (For interpretation of the references to colour in this figure legend, the reader is referred to the web version of this article.)

information regarding the potential subsurface conditions that exist at a specific site, taking into account the geological processes (Griffiths et al., 2012). The 2D ground model can enhance subsurface resolution to identify the slipping regions and characterize the triggering factors resulting in the slope instability for this research. Moreover, we also focus on the efficiency of geophysical techniques, which are 2D ERT and SRT in the landslide assessment. The results are attempted to identify the sliding plane and point out the landslide mechanism through a first conceptual ground model of unstable slopes at this site. Those two methods are used to clarify and show contrast between the landslide material and bedrock and indicate triggering of landslide in this study area. This approach applied first time in this landslide geological setting, where is relevant to mountainous areas impacted by monsoonal rainfall. This ground model is potential to be used as a first tool to study and monitor landslides in this region.

2. Geological description and climate conditions of study site

Nakhon Si Thammarat province is located in the southern Thailand (top left of Fig. 1). The study area of Thungsong districts is located at UTM Zone 47P 585250E 899365 N. The elevation of study area is approximately 150 and 180 m above mean sea level (Fig. 1). The hill slope angles are relatively steep at between 36 and 42 degrees. Fig. 1 shows the geological map of study site in Nakhon Si Thammarat province. The bedrock in this landslide is sandstone in the age of Cambrian (light green area marked 'E' in Fig. 1) covered by Quaternary deposits. There are many major landslides occurred in the old sedimentary rock due to high rate of weathering of sandstone and quartzite in this province.

A number of outcrops (orange circles in Fig. 1) have been surveyed as a component of this study to better understand the succession of the bedrock in this area. The Cambrian sandstone is called Talo Vow Formation, which is the part of Tarutao Group (DMR, 2014). The Talo Vow Formation comprises thin- to medium-bedded whitish-grey and greenish-grey quartzite (Fig. 2a) and well sorted with cross and graded bedding sandstone (Fig. 2b). The Talo Vow Formation is overlain by the Malaka Formation in the carbonate Thungsong Groups (dark green area marked 'O' in Fig. 1), which is a limestone of Ordovician age located in the south and other regions of Thailand (Bunopas, 1981). The Malaka Formation consists of muddy limestone interbedded with dolomitic limestone (Fig. 2c). The top of the Formation is grey mudstone interbedded with very fine-grained siltstone and sandstone (Fig. 2d). This

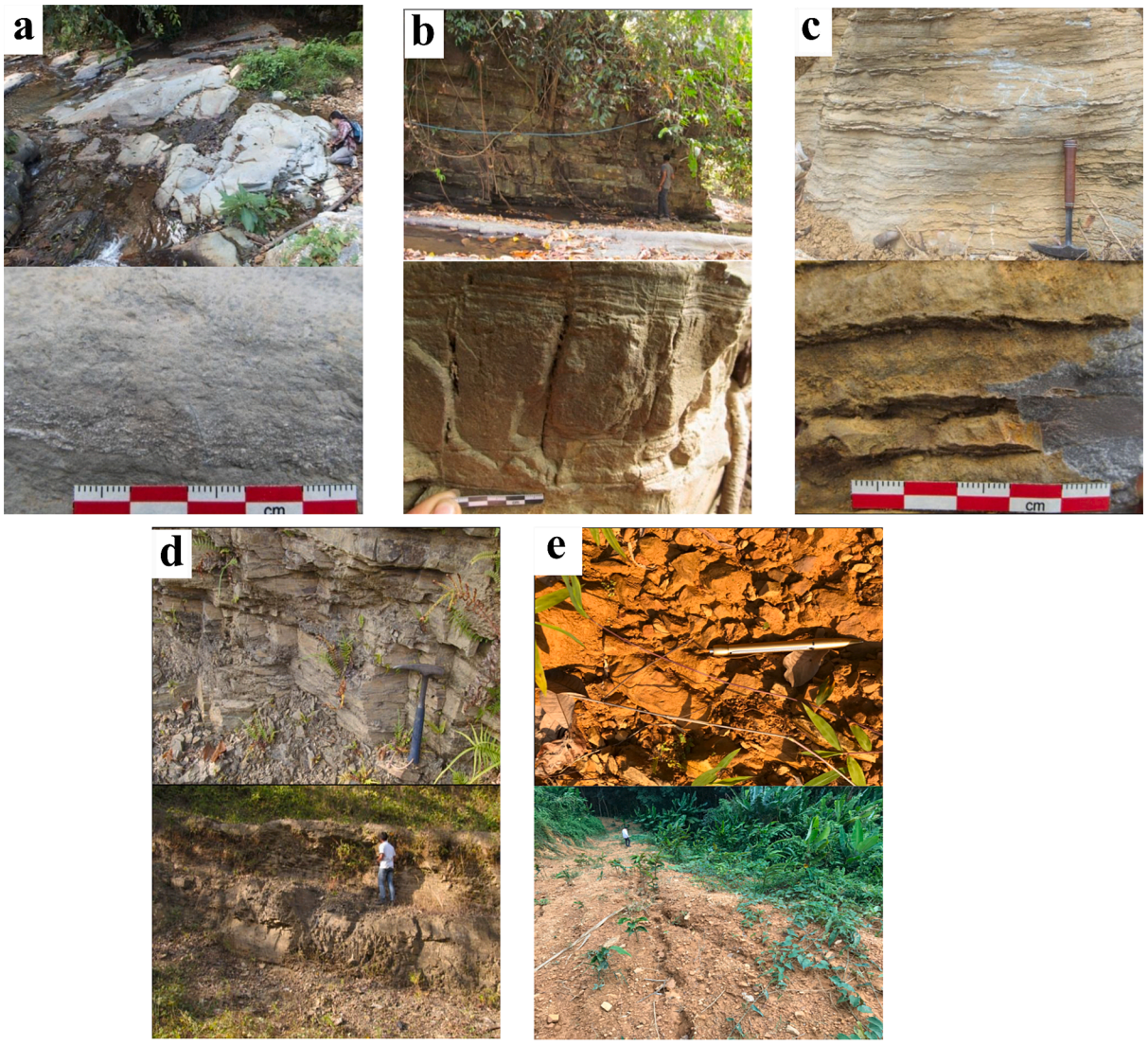

Fig. 2. Outcrops in this study area: a) thin- to medium-bedded whitish-grey and greenish-grey quartzite (outcrop number 1 in Fig. 1); b) cross and graded bedding sandstone(outcrop number 2 in Fig. 1); c) muddy limestone interbedded with dolomitic limestone (outcrop number 3 in Fig. 1); d) grey mudstone interbedded with very fine-grained siltstone and sandstone (outcrop number 4 in Fig. 1); e) colluvium sediments that are weathered sedimentary rocks, such as sand, clay, and various size of rock fragment..

layer shows highly weathering, which potentially leads to the landslide, acting as a sliding material.

The two Formations are covered by Quaternary colluvium (Fig. 2e), which is weathered from the bedrock and accumulated along the foothills of the mountains in the region. The colluvium deposits are mostly composed of weathered sedimentary rocks, related to the source of bedrocks. The deposits are therefore silt, clay, sand, gravel, and lateritic soil due to near a sandstone and limestone bedrocks. Furthermore, there is a borehole near the study area, drilled by Department of Groundwater Resources (DGR). It can help to better understand the lithology in study area (Table 1). The top layer is colluvium deposits, consisting of unconsolidated sediments with thickness of 1–3 m underlain by layer of sandy to silty clay of 3 m in thickness. The unconsolidated sediments are highly permeable, leading to easy infiltration to below silty clay layer, which is low permeability. This can make the subsurface susceptible to flow or slide on steep slopes. Under the colluvium lies a moderately weathered/fractured sandstone consisting of sand and gravel layer. This layer has approximately a thickness of 3 m and lies over a clay with weathered sandstone. Moreover, the groundwater table is in this layer. Beneath the moderately weathered/fractured layer is compact sandstone bedrock at a depth of approximately 16 m.

In addition to geological description, the study area is in a region of tropical monsoon characterized by high rain intensity with an annual precipitation of more than 2000 mm. This area is prone to rainfall-triggered landslides when the cumulative monthly rainfall intensity measured by Thailand Royal Irrigation Department in 2017 was close to 3500 mm (Fig. 3). Here, two landslides that were active in 2017 (light green circle in Fig. 1) are selected to study with the SRT and ERT methods. From the classification by Cruden and Varnes (1996), those two landslides can be categorized as shallow landslides accompanied by debris flow. These shallow landslides are the result of slip planes forming within the upper layers of the ground. The primary factors contributing to triggered landslides are rainfall seeping into the subsurface and rapidly increasing in the groundwater table level. Shallow failures occur along these slip planes when the moisture content approaches saturation due to cumulative rainfall, resulting in a dissipation of matric suctions and a decrease in soil strength (DMR report, 2014; Salee et al., 2022). The two landslides had occurred in sandstone bedrock covered by colluvium sediments. During land sliding the colluvium deposits had detached and displaced roughly 40 m from a main scarp (at the crown of the landslide) sliding down to base of slope. In this slope, two main scarps are located between 165 and 180 m in elevation with 36–42 degrees of steep slope angles (Fig. 4). The width of the larger main back scarps has an average of approximately 20 m compared to the another, which has a width of approximately 10 m. They have the same depth of sliding surface (approximately 3–5 m), categorized as shallow landslide at its middle (Fig. 4). The old cracks on the ground can be discovered on the top of the two main scarps. At the toe of these two main scarps, there are a lot of sliding materials with the colluvium deposits, such as sand mixed with clay, silt, lateritic soil, and displaced rock fragments.

Table 1
Description of lithology of the borehole nearby the study area drilled by DGR.

Explanation	Depth
Layer1: Colluvium deposits	
Unconsolidated sediments: dry sand, gravel, silt and laterite	0–3 *m*
Sandy to silty clay	3–6 *m*
Layer2: Moderately weathered bedrock	
Consolidated sediments, such as sand and gravel	6–9 *m*
Grey clay and the groundwater can be found	9–16 *m*
Layer3: Bedrock	
Sandstone	Beneath 16 *m*

3. Materials and methods

The ERT and P-wave SRT surveys were acquired in the study area along with four longitudinal profiles (line 1, line 2, line 3, line 4), trending in NE to SW direction. Line 1 and line 4 overlie the landslide areas in the past. They are pseudo-parallel to line 2 and line 3. Line BH is a survey line near the borehole, located at UTM 47P 586600E 900613 N, approximately 600 m from the 4 profiles at the study area (Fig. 4). Line BH is used as a survey calibration with lithological borehole data.

3.1. ERT measurements

The 2D ERT data was collected using 61 electrodes with the dipole–dipole array by the ABEM Lund imaging system (Fig. 5a). The ABEM Terrameter SAS1000 was connected to the switching unit to automatically select the four electrodes for each measurement (Fig. 5a). The 61 electrodes were deployed with 3 m spacing and dipole sizes (n) of 1 to 6. The length of each profile was 180 m. The data processing was conducted using the RES2DINV produced by Geotomo Software. The steps of data processing are based on Loke and Barker (1996) to image 2D true resistivity model through an inversion process. The bad datum points were removed before the inversion step. They are identified as outliers due to bad contact between electrodes and the ground surface (very dry soil and rock). The elevation data from field measurement was also included to the processing. In the inversion step, the apparent resistivity data was transformed into a true resistivity model with depth of the subsurface. The inversion algorithm selected in this study is robust or blocky inversion method (L_1-norm), which is less sensitive to noisy data (Loke et al., 2003). An RMS error is assessed in each step in the inversion. The damping factor is important to stabilize inversion. Therefore, the suitable damping factors were applied to noisy data or less noise data, respectively. All inversions are converged after ten iterations.

3.2. P- wave SRT measurements

The P-wave SRT method was employed along each profile. The seismic data was recorded by the Smartest S-24 seismograph with 24 channels. The vertical twenty-four geophones with a natural frequency of 14 Hz were deployed with 3 m spacing. A 10 kg sledge hammer was used as the energy source with shot spacing of 6 m (Fig. 5b). To improve signal to noise ratio, every shot point (star symbol in Fig. 4) was stacked 5 times. Each shot point was recorded a total time of 512 ms with the sampling rate of 0.25 ms. The total length of each profile was 141 m. The layout of four profiles were operated in 3 spreads extending each spread of 69 m and 2 overlaps of 33 m (Fig. 5b). To process the SRT data, the SeisImager2D software package (OYO Corporation, 2004) was used. There are two modules for SRT data processing in this software. The first step is to pick first arrival times of P-waves, using the Pickwin program. The second step is inversion to velocity model with depth of the subsurface, using the Plotrefa program. Before picking first arrival time, the noise signals from traffic and wind were removed by frequency filter. A gain control was also applied to amplify and enhance the visibility of the seismic data. Subsequently, the first arrival times of recorded P-waves were picked in each shot point to obtain time-distance (t-x) curve by the Pickwin program. The t-x curves were inverted to a velocity model by inversion using the Plotrefa program.

The SRT inversion begins to generate an initial velocity model. The initial model can be created by time-term inversion and assigned parameters from the first arrival travel time curve. The cell sizes of the initial model are larger at deeper depths than those near surface (Sheehan et al., 2005). The inversion step involves the use of non-linear least-squares method and wave front propagation ray tracing for the travel time modelling (OYO, 2004). The horizontal and vertical smoothing parameters were also modified during the inversion process. The ray tracing through the model calculates travel times. The calculated travel times were compared to the measured travel times. An RMS

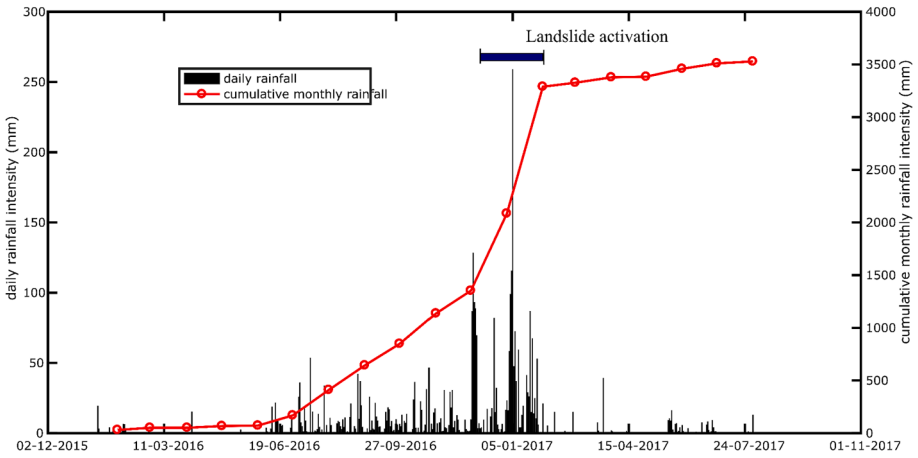

Fig. 3. Daily and cumulative monthly distribution of rainfalls at Thungsong in 2016–2017.

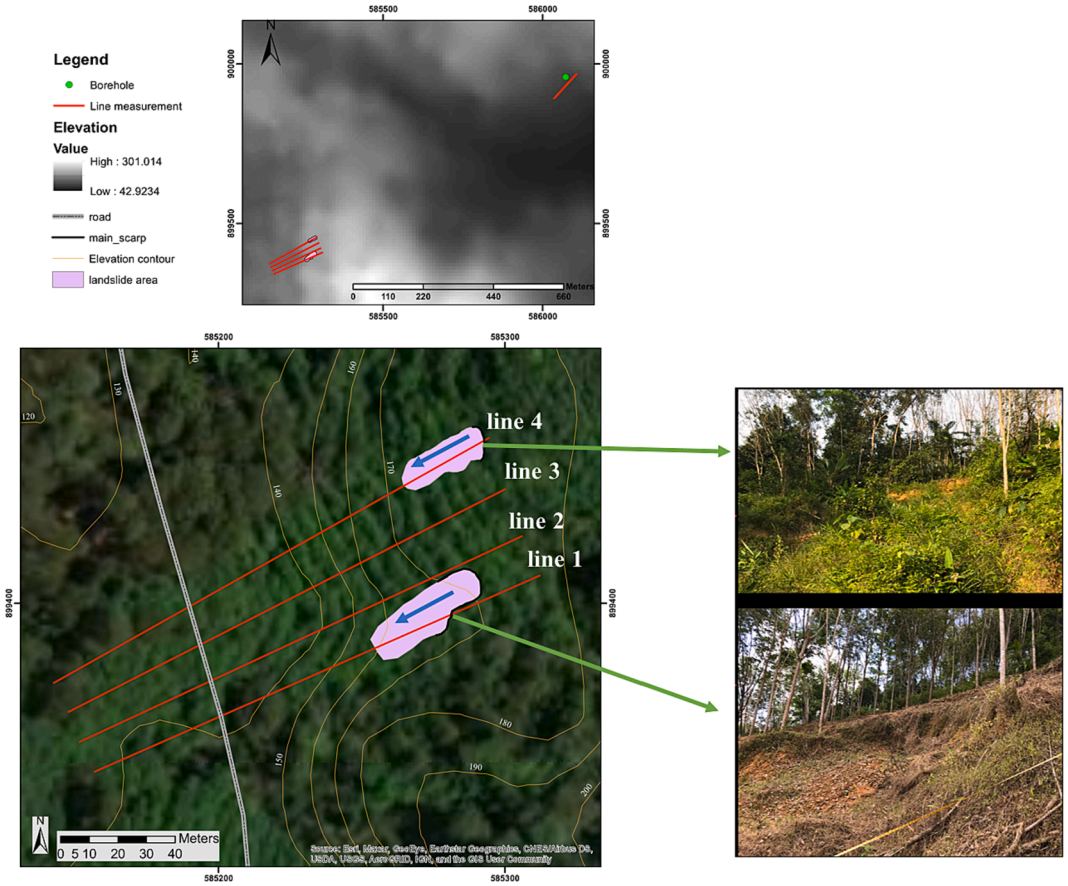

Fig. 4. Map and plan of the geophysical survey at the study site with two main back scarps in the study area, where landslides occurred.

value is expressed by their differences between the measured and calculated travel times. The model was perturbed iteratively until the difference between the measured and calculated travel times is minimized.

4. Results

The inversion results and interpretation of ERT and SRT are shown for 4 profiles (line 1, line 2, line 3, and line 4) in this section. Moreover, the inversion models in line BH is also presented as a calibration and validation model with real lithological data from borehole. The location of each profile is shown in Fig. 4.

4.1. 2D ERT and P-wave SRT models for the line BH

The ERT and P-wave SRT profiles were surveyed near the borehole (see Fig. 4f or location). The purpose is to calibrate and interpret the values of resistivity and P-wave velocity for four profiles in the study area. The length of line BH was 112 for ERT and was 105 m for SRT. The P-wave SRT and ERT inversion models are overlain and correlated with the borehole descriptions (Figs. 6 and 7). The model interpretations are related to the borehole lithology in Table 1 and resistivity and P-wave

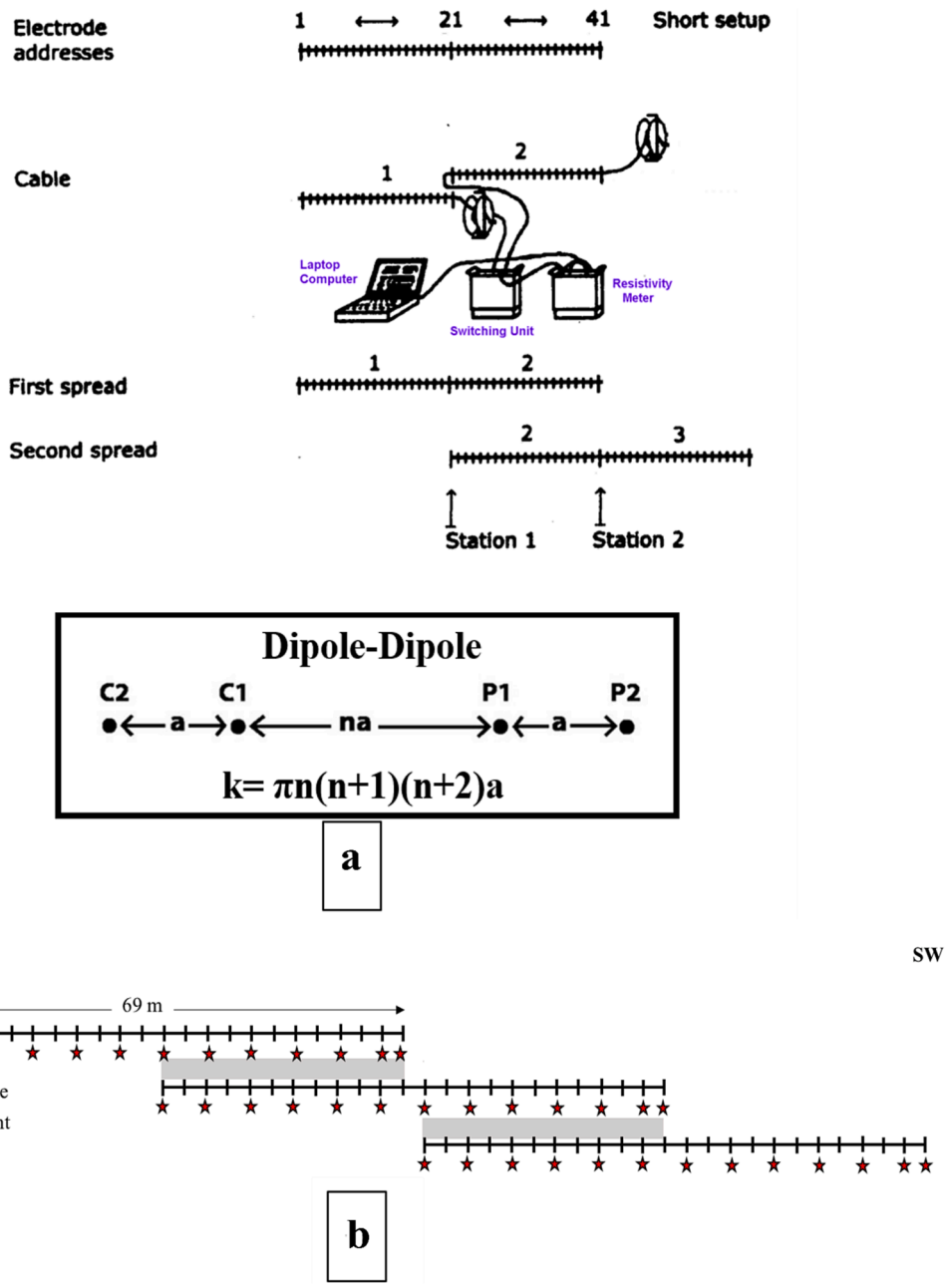

Fig. 5. The data acquisition in this site: a) layout of the 2D ERT using ABEM Lund imaging System (Loke, 2001); b) layout of the 2D SRT data acquisition.

velocity values of earth material from other publications. The P-wave SRT results with RMS value of 1.5 ms are correlated with the lithology from the borehole (Fig. 6a). The model depth is approximately 20 m. The P-wave SRT inversion model is converted to a layer model (Fig. 6b). Three zones of different velocities can be interpreted into three layers (Fig. 6b). The top layer reveals a relatively low P-wave velocity in a range of 300–900 m/s. The thickness of this layer varies from a few to 5 m. This layer is interpreted as unconsolidated colluvium deposits, which are dry sand and gravel, silt, sandy to silty clay, and highly weathered sandstone. The second layer shows the intermediate P-wave velocity varying from 900 to 1800 m/s with thickness of approximately 9 m. The P-wave velocity increases in this layer due to more compact sediments, which is correlated to moderately weathered sandstone layer in the borehole. The bottom layer has relatively high P-wave velocities of more than 1800 m/s. This layer is interpreted as consolidated sandstone.

Fig. 7a reveals the ERT inversion model with RMS error of 5.5 % correlated with the borehole lithology. In general, the relatively low resistivity values are associated with higher moisture or clay content, while relatively high resistivity values are associated with dry sediments with less clay or lower water content, such as dry sand, and dry weathered and fractured sandstone. The ERT inversion model is divided to 3 layers based on the P-wave SRT layer model (Fig. 7b). The colluvium deposits in the top layer show a variation of resistivity values, likely reflecting variations in clay and water content. The relatively low resistivity values in a range of 60 to 250 Ωm are correlated to sandy to silty clay in the borehole lithology. In contrast, the relatively high resistivity values in a range of 630 to 2500 Ωm are consistent with dry and unconsolidated sediments, such as dry sand, lateritic soil, and dry sandstone fragments. At greater depth, relatively intermediate to high resistivity values in a range of 630 to 1500 Ωm are interpreted as moderately weathered sandstone layer (sand and gravel). On the other hand, the relatively low resistivity values (60–250 Ωm) are interpreted as the grey clay with groundwater table. The bottom layer reveals very high resistivity values greater than 1500 Ωm. As a result, the range of

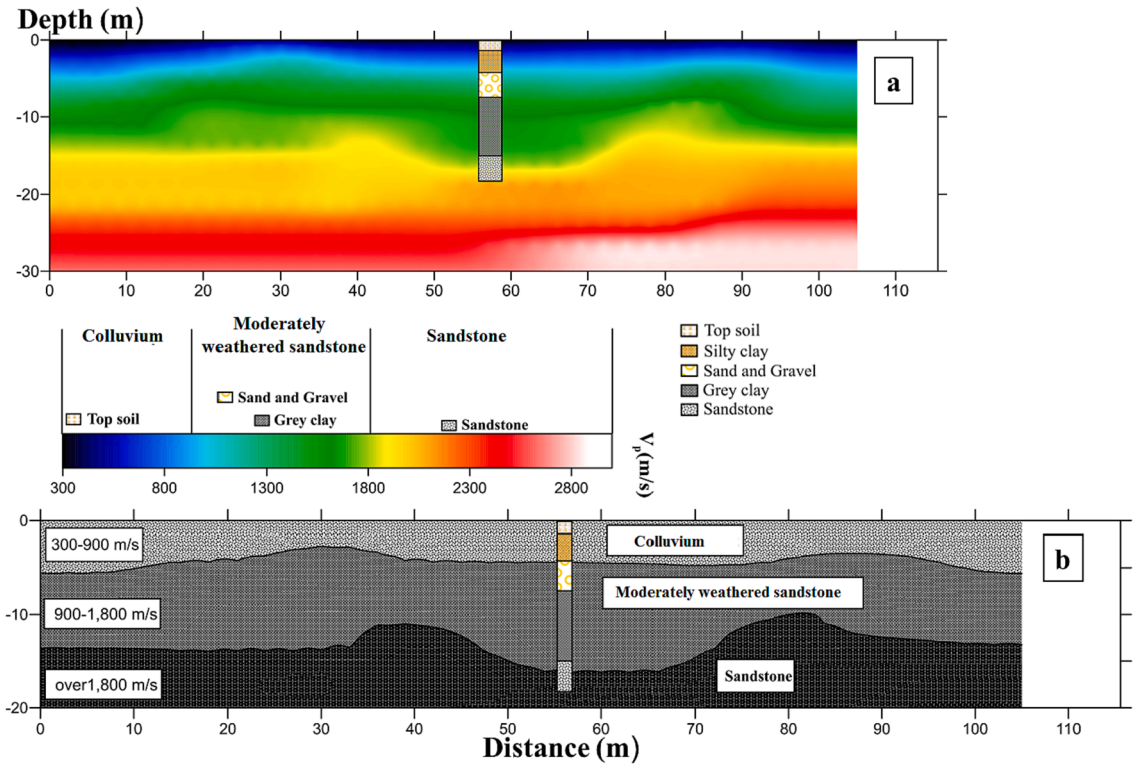

Fig. 6. The SRT results obtained along line BH: a) P-wave SRT inversion model overlain and correlated with borehole descriptions b) the layered model with interpretation of three layers of different P-wave velocities.

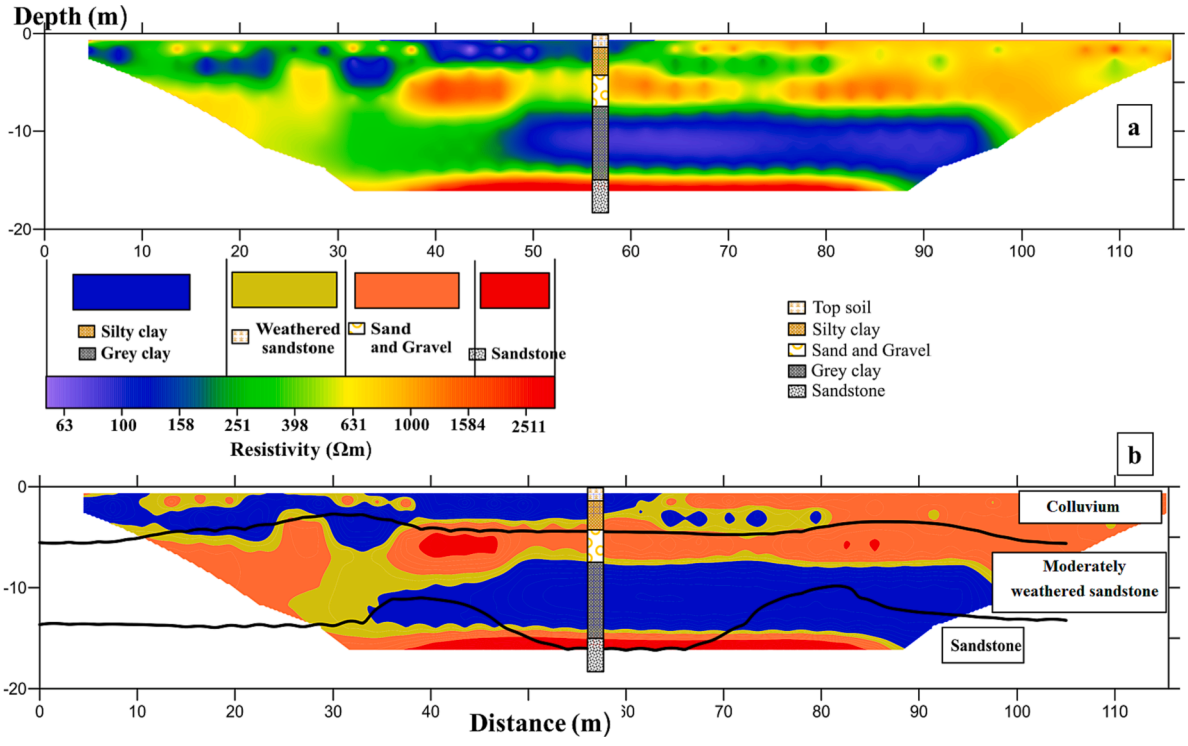

Fig. 7. The ERT results for the line BH: a) 2D electrical resistivity model overlain and correlated with borehole descriptions b) model of resistivity interpretation with different resistivity values and boundaries of black line from the SRT model.

resistivity value from the inversion model can classify the lithology in this study area as presented in Fig. 7b. The resistivity values ranging from 60 to 250 Ωm are assorted to silty clay and grey clay (dark blue colour). The resistivity values ranging from 630 to 1500 Ωm are assorted to sand and gravel and moderately fractured sandstone (orange colour). The resistivity values over 1500 Ωm are assorted to less weathered and fractured sandstone (red colour). Consequently, the above results show the powerful use of resistivity and seismic data jointly. The P-wave SRT

results obviously show the lithological layers that increase in compaction with depth, such as unconsolidated sediments to moderately weathered rock, to compact bedrock. The resistivity value is more sensitive to water and clay content. Therefore, the ERT results show a better interpretation of soil and rock type in lateral variations due to clay and water content. Next the information obtained from the line BH is used to interpret the P-wave SRT and ERT data along the four profiles in the study area.

4.2. P-wave SRT landslide survey results

All profiles trend in NE to SW direction (see Fig. 3). The length of each P-wave SRT model is 141 m. Lines 1 and 4 were positioned on the landslide scar occurred in 2017. The sliding areas lie at the distances between 23 m and 68 m for line 1 and the distance between 3 m and 26 m from the for line 4 (Fig. 4). The SRT inversion produced four P-wave SRT models shown in Fig. 8, with an absolute RMS error of 3.1, 2.3, 2.2, and 3.0 ms for line 1, 2, 3, and 4, respectively. These tomographic models are interpreted by the borehole calibration in section 4.1 and converted to four P-wave velocity layer models shown in Fig. 9.

The layered models for all profiles reveal three layers. The top layer reveals P-wave velocity in the range of 300 m/s to 900 m/s, interpreted as colluvium deposits. The depth of this layer differs from 0 m to 5 m, thicker towards the base of slope. This layer is the main sliding material corresponding with failure at the main scarp and a steep angle in the top of the slope. The main sliding materials slipped approximately 50 m downslope from the crown of this landslide (a visible scarp) downward to the base of slope in line 1 and a distance of approximately 30 m in line 4 (Fig. 9). Under the colluvium layer shows the P-wave velocities ranging from 900 m/s to 1800 m/s, interpreted as moderately weathered sandstone. The bottom layer is interpreted as sandstone with P-wave velocities more than 1800 m/s. The moderately weathered sandstone and sandstone layer attach to the surface near the top of slope. In the landslide area (lines1 and 4), the slope angle of sandstone bedrock is remarkably steep at the back scarp. This can result in landslide activation. The depth of surface of rapture in line 1 and 4 is approximately 2–3 m.

4.3. ERT landslide survey results

The ERT models for each profile are shown in Fig. 10 with the length of 180 m. The RMS errors for each profile are 6.6, 7.7, 7.2, and 4.5 % for lines 1, 2, 3, and 4, respectively. The interpretation of these models from lithology and the results from the line BH is shown in Fig. 11. The ERT inversion model is divided into three layers based on SRT result (Fig. 11). The colluvium layer reveals relatively low resistivity values in the range of 60 to 250 Ωm) at the top of slope particularly in landslide area (line 1 and line 4). This low resistivity value is interpreted as moist sandy to silty clay with low porosity. In contrast the relatively high resistivity value in the range of 630 to 2500 Ωm at base of the slope are interpreted as dry unconsolidated materials, such as dry sand, lateritic soil, and weathered sandstone fragments with high porosity. The clay zones in line 1 and line 4 are consistent with the landslide material related to the position of landslide event. The layer below is the moderately weathered sandstone. The middle and base of the slope of this layer (distance between 45 and 140 m) reveal low resistivity zones (less than 250 Ωm). This is interpreted as silty clay to grey clay with the saturated zone. In contrast, the relatively high resistivity zone (more than 650 Ωm) at the top of the slope indicates moderately weathered sandstone with low water and clay content or sand and gravel layer. This layer is close to bottom layer that shows very high resistivity value (over 1500 Ωm). This bottom layer is interpreted as sandstone bedrock that can be found only at the top of slope.

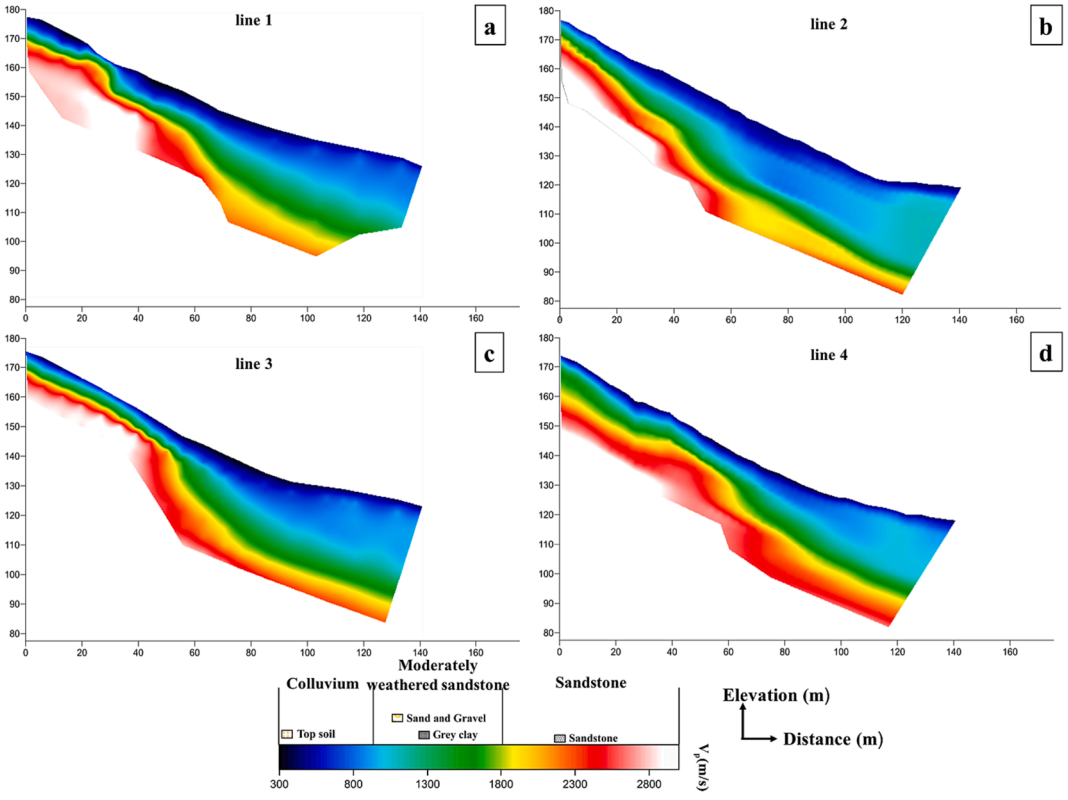

Fig. 8. SRT inversion models for: a) line 1b) line 2c) line 3 d) line 4.

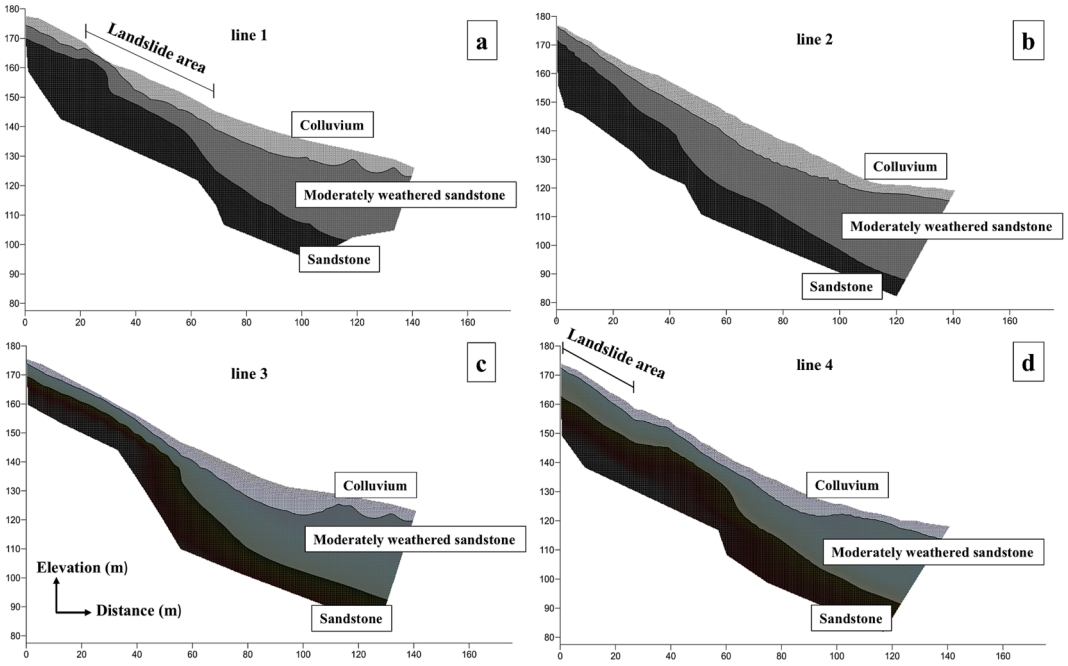

Fig. 9. Layer models correlated with lithology inferred from the line BH for: a) line 1b) line 2c) line 3 d) line 4.

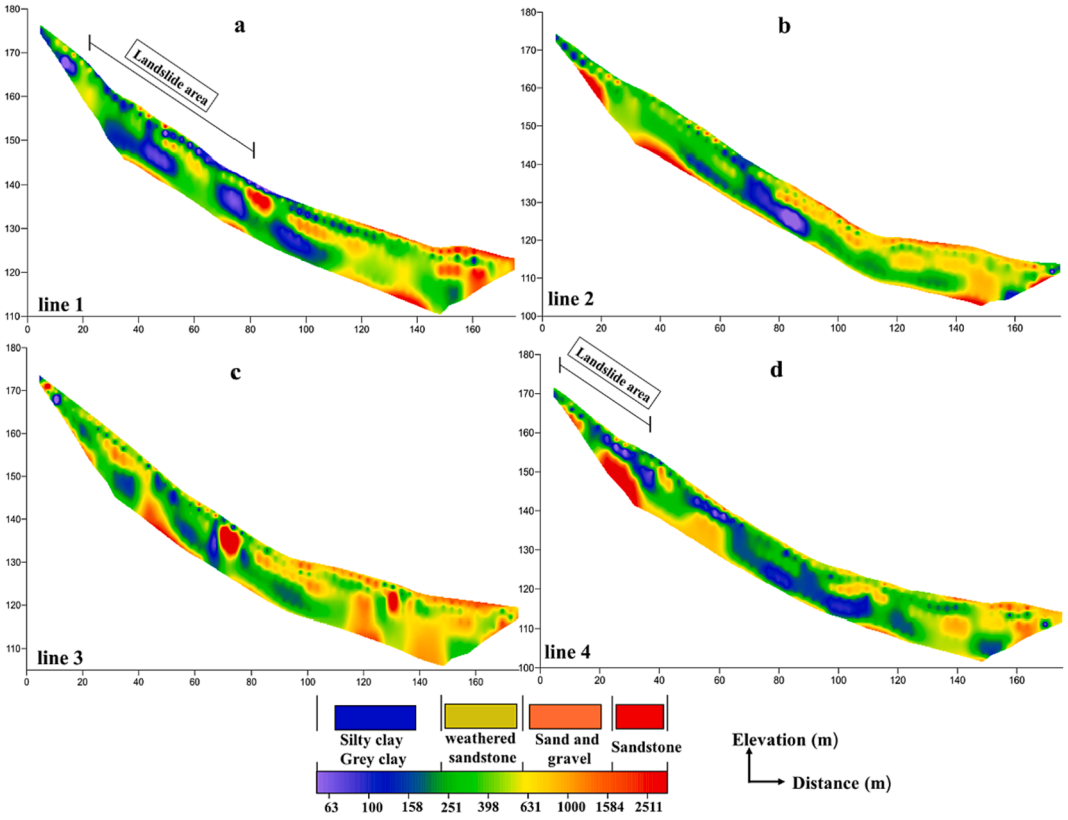

Fig. 10. ERT inversion models for: a) line 1b) line 2c) line 3 d) line 4.

5. Discussion

5.1. Correlation between P-wave SRT, ERT, and geological features in this landslide site

The joint integration of the ERT and SRT results for four profiles is presented in 3D view model (Fig. 12). This 3D view model illustrated by the 2D results gives better information to assess the landslide structure in the study site. The resistivity and velocity values of lithological structure are compared and calibrated with the values obtained from the borehole (line BH).

The geological structures in this site is separated in three main layers

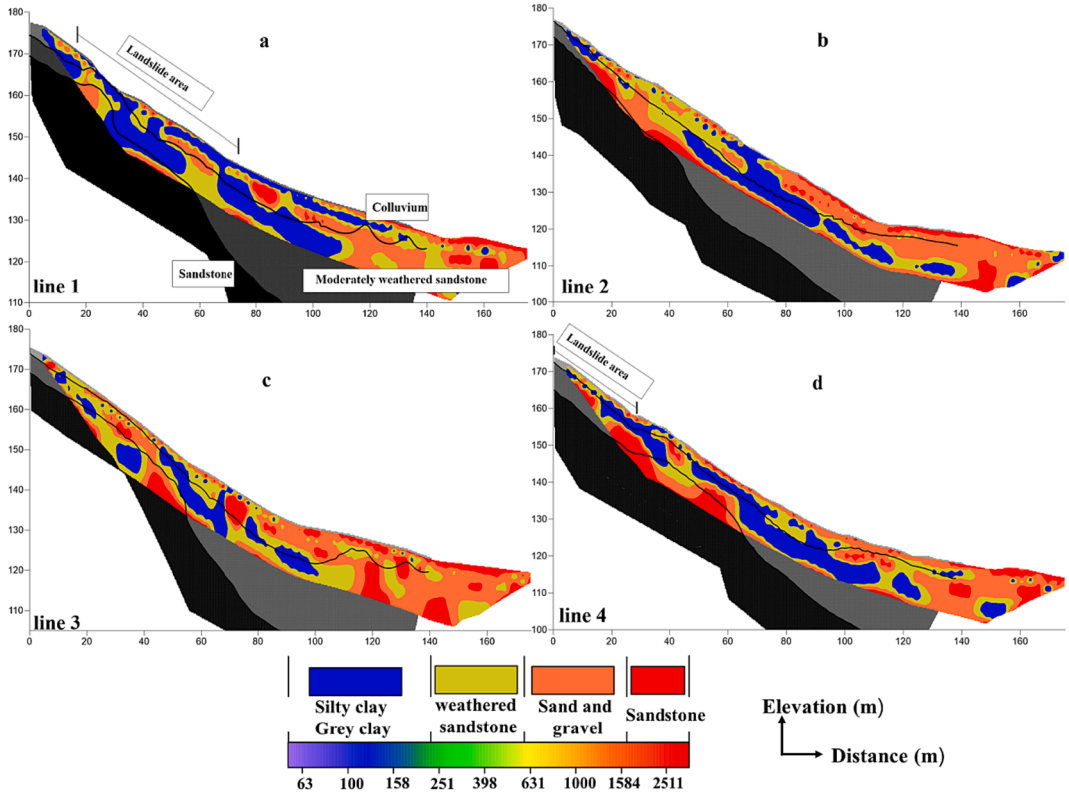

Fig. 11. ERT results correlated with SRT layer model and lithology inferred from the Borehole Line for: a) line 1b) line 2c) line 3 d) line 4.

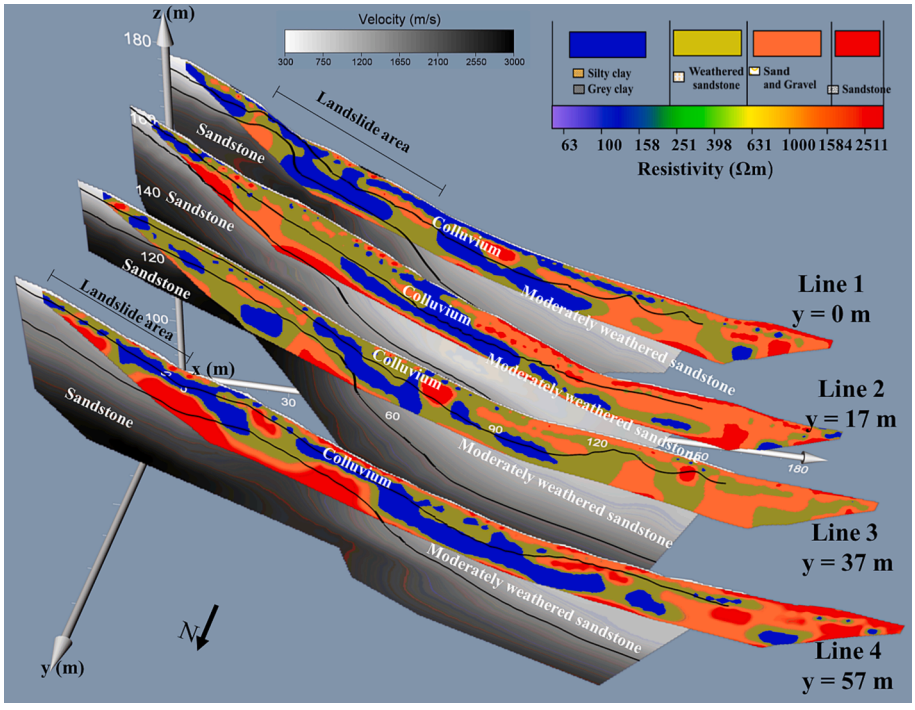

Fig. 12. Vertical sections of combined ERT and SRT results for lines 1–4. Geologic features based on the ERT interpretation are shown as the colour areas. The geological boundaries (black lines) are based on the SRT interpretation.

(black line in Fig. 12) as derived from the SRT images. The top layer reveals relatively low velocities (300–900 m/s), indicating colluvium. The below layer is moderately weathered/fractured sandstone with higher velocities (900–1800 m/s). This indicates a more compact layer consisting of sand, gravel, and grey clay. The bottom layer reveals relatively high P-wave velocities (over 1800 m/s), indicating the sandstone bedrock. The ERT method then provides evidence of geological variations in the lateral direction. The resistivity values are separated into three groups: the first group has relatively low resistivity values (blue colours in Fig. 12), indicating high clay and water content; the

second group has higher resistivity values (green and orange colours in Fig. 12), indicating dry top soil and moderately weathered sandstone; the last group has very high resistivity (red colours in Fig. 12), indicating sandstone bedrock. The various amounts of clay content in the top of slope are different in each profile. Lines 1 and 4 indicate contribution in sliding materials due to the presence of high clay contents, while there are less clay contents in the top of slope for lines 2 and 3, which have no sliding mass. Next a conceptual ground model of landslide in this site is produced by an integration of the SRT and ERT results (Fig. 13).

5.2. Joint interpretation of the results leading to conceptual model of Thungsong landslide

This ground model is divided into three zones and six lithological units (colour areas in Fig. 13) related to the ERT and SRT results and the borehole lithology.

5.2.1. Zone 1

Zone1 covers the top of the slope (distance from 0 to 65 m), where the slope angle is relatively steep (greater than 40 degrees). The black area is sandstone bedrock, which is shallow and visually observed in outcrop in this zone. The sandstone bedrock has relatively high resistivity values (more than 1500 Ωm) and P-wave velocities (more than 1800 m/s). Over the sandstone bedrock is the colluvium sediments, consisting of silty clay (dark blue area) and top soil (grey area). The top soil is very dry unconsolidated materials near the surface related to relatively high resistivity values (over 630 Ωm) and very low seismic velocities (less than 450 m/s). The silty clay reveals relatively low resistivity values in a range of 60–250 Ωm. This zone covers the landslide areas in lines 1 and 4. The sliding material is due to relatively steep slopes and high silty clay volume in the landslide area. The sliding material is colluvium sediment with variable thicknesses from 2 to 5 m. The slip surface (yellow dash line in Fig. 13) is visible in the back scarps at line 1 and line 4, and represents the January 2017 landslide events associated with torrential rainfall (cumulative monthly rainfall of over 3500 mm, as measured by Thailand Royal Irrigation Department (2017), see Fig. 3). The silty clay layer is the main causes of slipping in this zone. This is due to saturation in the silty clay layer during torrential rainfall. Moreover, there are a lot of cracks in the top soil layer. This is easy to water infiltration, leading to high pore-water pressures (black arrow in Fig. 13). Consequently, the shear stress increases, while the shear strength decreases in the silty clay layer. This leads to the subsurface susceptible to move or slide downward the steep slopes. Furthermore, lines 1 and 4 also exhibit much more extensive silty clay in Zone 1, which could explain why there is no sliding mass in lines 2 and 3 (see Fig. 12).

5.2.2. Zone 2

Zone2 lies in the middle of the slope (between 65 m and 127 m) and reveals large area of moderately to less weathered sandstone (red area in Fig. 13) over sandstone bedrock. This moderately to less weathered sandstone shows intermediate value of P-wave velocity (900–1800 m/s). This layer consists of compact sand and gravel (orange area in Fig. 13) and grey clay containing groundwater (light blue area in Fig. 13). The groundwater flows from the top of the slope and infiltrates downwards from the above layers. The grey clay and groundwater shows relatively low resistivity (60–250 Ωm), while sand and gravel layer reveals relatively high resistivity (more than 650 Ωm). Moreover, the top layer of this zone is indicative of the dry colluvium deposits with relatively high resistivity (over 600 Ωm), and very low P-wave velocity (less than 450 m/s). Although silty clay volume can be found in the colluvium layer of this zone, it is much less extensive than zone 1.

5.2.3. Zone 3

Zone 3 lies below the toe of the slope (distance from 127 m to 170 m). The top layer is colluvium deposits characterised by relatively high resistivity values (more than 600 Ωm) but relatively low P-wave velocities (less than 450 m/s). The layer in this zone contains very dry poorly unconsolidated materials with less silty clay contents. Under this layer is the moderately weathered sandstone with sand and gravel. Dissimilar to zone 2, there is much less evidence of deeper clays and a water table in the zone. The layer of sandstone bedrock is relatively deep and barely found in this zone.

In summary, this ground model points out the significant difference between the sliding material and the stable bedrock in this landslide. It also delineates the zones of high clay content and shallow sandstone bedrock in the sliding regions at the top of the slopes. The significant variations are apparent between lines; in particular, the regions of landslides on lines 1 and 4 are present higher volumes of silty clay in the colluvium deposits than observed in lines 2 and 3. This silty clay layer combined with a number of cracks in the top soil is the main reason of slipping in this study area, because the water is easy to percolate through the cracks, leading to high pore-water pressures saturation of the silty clay during intensive rainfall. This process leads to reduce the shear strength and friction between subsurface particles. The saturated silty clay together with unconsolidated colluvium begins moving downwards the slope.

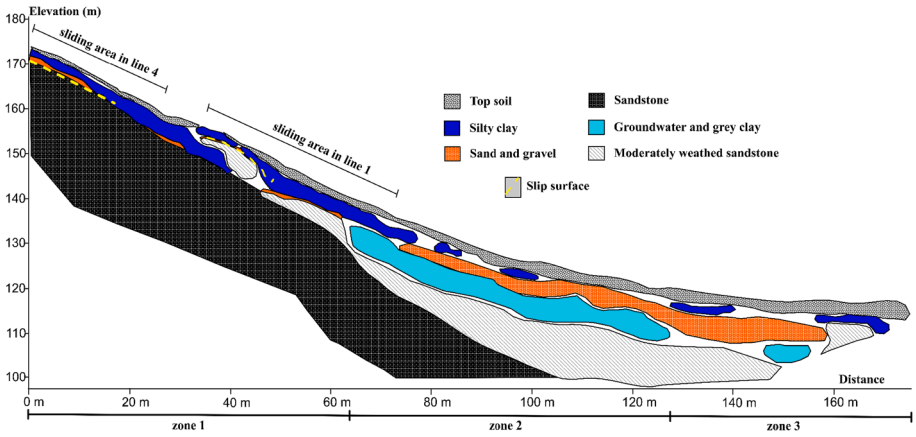

Fig. 13. Conceptual ground model of landslide in this study area is developed from joint interpretation of the geological results. The model is divided into three zone and six geological features. The yellow dashed lines and the black arrows indicate slip surfaces and water movement. (For interpretation of the references to colour in this figure legend, the reader is referred to the web version of this article.)

6. Conclusions

A detailed ground model produced from the combination of SRT and ERT results together with geological data has shown reliable information in terms of the subsurface structures and landslide mechanisms for the study area. The joint integration of ERT and SRT results is useful to reduce ambiguities in interpretation of the geophysical data. The SRT method delineates the model of geological layers associated with the variations in seismic velocities, while the ERT method indicates the shape of the surface rupture and shows lateral variations and thickness of the sliding material, related to moisture and clay contents. The ERT method can also reveal the groundwater contents in various layers in the subsurface. By integrating these two methods, the limitations of each method can be mitigated. The synergistic use of these two methods proves valuable in reducing the reliance on extensive borehole investigations and is crucial to obtain a comprehensive understanding of detailed stratigraphic sequences with landslide ground model. This model can use as a primary implement for landslide investigation and monitoring in this area and provides a conceptual understanding of the slope. This is a key element of landslide early warning system design and used to develop a plan of landslide protection, such as engineering solutions and road barriers.

Declaration of competing interest

The authors declare that they have no known competing financial interests or personal relationships that could have appeared to influence the work reported in this paper.

Data availability

Data will be made available on request.

Acknowledgments

I would like to thank Prof. Michael Kendall, head of geophysics research in school of Earth Science, University of Oxford for his guidance and suggestion in the geophysical results, discussion, and feedbacks to my writing. I would like to thanks to Prof. Jonathan Chambers from British Geological Survey (BGS), for his suggestions and comments for geophysical results. I would like to thank the Geophysics Research Centre (GRC), Department of Physics, Faculty of Science, Prince of Songkla University in Thailand to support geophysical equipment for fieldwork. I would like to thank GRC team for their help during fieldwork.

References

Asriza, Supriyanto, Kristyanto, T.H.W., Indra, T.L., Syahputra, R. and Tempessy, A.S., 2017. Determination of the landslide slip surface using electrical resistivity tomography (ERT) technique. In Advancing Culture of Living with Landslides: Volume 2 Advances in Landslide Science (pp. 53-60). Springer International Publishing.

Bunopas, S., 1981. Paleogeographic history of western Thailand and adjacent parts of Southeast Asia - A plate tectonics interpretation: Victoria University of Willington, unpublished Ph.D. thesis, 810 p.; reprinted 1982 as Geological Survey Paper no.5, Geological Survey Division, Department of Mineral Resources, Bangkok, Thailand.

Capizzi, P., Martorana, R., 2014. Integration of constrained electrical and seismic tomographies to study the landslide affecting the cathedral of Agrigento. J. Geophys. Eng. 11 (4).

Chambers, J.E., Wilkinson, P.B., Kuras, O., Ford, J.R., Gunn, D.A., Meldrum, P.I., Pennington, C.V.L., Weller, A.L., Hobbs, P.R.N., Ogilvy, R.D., 2011. Three-dimensional geophysical anatomy of an active landslide in Lias Group mudrocks, Cleveland Basin, UK. Geomorphology 125, 472–484.

Chen, Q., Zhang, S., Chang, S., Liu, B., Liu, J., Long, J., 2019. Geophysical interpretation of a subsurface landslide in the Southern Qinshui Basin. J. Environ. Eng. Geophys. 24 (3), 433–449.

Colangelo, G., Lapenna, V., Perrone, A., Piscitelli, S., Telesca, L., 2006. 2D Self-potential tomography for studying groundwater flows in the Varco d'Izzo landslide (Basilicata, southern Italy). Eng. Geol. 88 (3–4), 274–286.

Confuorto, P., Di Martire, D., Centolanza, G., Iglesias, R., Mallorqui, J.J., Novellino, A., Plank, S., Ramondini, M., Thuro, K., Calcaterra, D., 2017. Post-failure evolution analysis of a rainfall-triggered landslide by multi-temporal interferometry SAR approaches integrated with geotechnical analysis. Remote Sens. Environ. 188, 51–72.

Cruden, D.M., Varnes, D.J., 1996. Landslide types and processes. In: AK, T., Schuster, R. L. (Eds.), Landslides: Investigation and Mitigation Spec. Rep. 247 36–75.

de Bari, C., Lapenna, V., Perrone, A., Puglisi, C., Sdao, F., 2011. Digital photogrammetric analysis and electrical resistivity tomography for investigating the Picerno landslide (Basilicata region, southern Italy). Geomorphology 133 (1), 34–46.

Department of Mineral Resources., 2014. Geology of Thailand. Department of Mineral Resources, Ministry of Natural Resources and Environment, Bangkok, Thailand, 508 p.

Dijkstra, T., Dixon, N., Crosby, C., Frost, M., Gunn, D., Fleming, P., Wilks, J., Uk, C., 2014. Forecasting infrastructure resilience to climate change. Proc. Inst. Civ. Eng, 167, 269–280.

Falae, P.O., Kanungo, D.P., Chauhan, P.K.S., Dash, R.K., 2019. Electrical resistivity tomography (ERT) based subsurface characterisation of Pakhi Landslide, Garhwal Himalayas, India. Environ. Earth Sci. 78, 1–18.

Fell, R., Hungr, O., Leroueil, S., Riemer, W., 2000. Keynote paper – Geotechnical engineering the stability of natural slopes and cuts and fills in soil. In: – in: Proc. Geoeng2000, Int. conf.on Geotechnical and Geol. Eng in Melbourne, Australia, Vol 1. Technomic Publishing, Lancaster, pp. 21–120. ISBN: 1-58716-067-6.

Gance, J., Sailhac, P., Malet, J.-P., 2014. Corrections of surface fissure effect on apparent resistivity measurements. Geophys. J. Int. 200 (2), 1118–1135.

Gariano, S.L., Guzzetti, F., 2016. Landslides in a changing climate. Earth Sci. Rev. 162, 227–252.

Glendinning, S., Hughes, P., Helm, P., Chambers, J., Mendes, J., Gunn, D., Wilkinson, P., Uhlemann, S., 2014. Construction, management and maintenance of embankments used for road and rail infrastructure: implications of weather induced pore water pressures. Acta Geotech 9, 799–816.

Griffiths, J., Stokes, M., Stead, D., Giles, D., 2012. Landscape evolution and engineering geology: results from IAEG Commission 22. Bull Eng Geol Environ 71, 605–636.

Gunn, D.A., Chambers, J.E., Hobbs, P.R.N., Ford, J.R., Wilkinson, P.B., Jenkins, G.O., Merritt, A., 2013. Rapid observations to guide the design of systems for long-term monitoring of a complex landslide in the Upper Lias clays of North Yorkshire. UK. q. J. Eng. Geohydrology 46, 323–336.

Imani, P., Tian, G., Hadiloo, S., El-Raouf, A.A., 2021. Application of combined electrical resistivity tomography (ERT) and seismic refraction tomography (SRT) methods to investigate Xiaoshan Distric landslide site: Hangzhou, China. J. Appl. Geophys. 184.

Jongmans, D., Garambois, S., 2007. Geophysical investigation of landslides: a review. Bull. Soc. Géol. Fr 33, 101–112.

Loke, M.H., Barker, R.D., 1996. Rapid Least-Squares Inversion of Apparent Resistivity Pseudosections by a Quasi-Newton Method. Geophys. Prospect. 44, 131–152.

Loke, M.H., Acworth, I., Dahlin, T., 2003. A comparison of smooth and blocky inversion methods 2-D electrical imaging surveys. Explor. Geophys. 34 (3), 182–187.

Loke, M.H., 2001. Electrical imaging surveys for environmental and engineering studies. A practical guide to 2-D and 3-D surveys, RES2DINV Manual.

Ma, Z., Mei, G., Piccialli, F., 2021. Machine learning for landslides prevention: a survey. Neural Comput & Applic 33, 10881–10907.

McCann, D.M., Forster, A., 1990. Reconnaissance geophysical methods in landslide investigations. Eng. Geol. 29 (1), 59–78.

Merritt, A.J., Chambers, J.E., Murphy, W., Wilkinson, P.B., West, L.J., Gunn, D.a., Meldrum, P.I., Kirkham, M., Dixon, N., 2013. 3D ground model development for an active landslide in Lias mudrocks using geophysical, remote sensing and geotechnical methods. Landslides, 11, 537–550.

Morelli, S., Utili, S., Pazzi, V., Castellanza, R., Fan, X., 2019. Landslides and geophysical investigations: Advantages and limitations. Int. J, Geophys, p. 2019.

OYO Corporation., 2004. SeisImager2D manual version 3.0.

Perrone, A., Lapenna, V., Piscitelli, S., 2014. Electrical resistivity tomography technique for landslide investigation: a review. Earth Sci. Rev. 135, 65–82.

Reichenbach, P., Busca, C., Mondini, A.C., Rossi, M., 2014. The Influence of Land Use Change on Landslide Susceptibility Zonation: The Briga Catchment Test Site (Messina, Italy). Environmental Management 54, 1372–1384 (2014).

Rezaei, S., Shooshpasha, I., Rezaei, H., 2019. Reconstruction of landslide model from ERT, geotechnical, and field data, nargeschal landslide. Iran. Bulletin of Engineering Geology and the Environment 78, 3223–3237.

Salee, R., Chinkulkijniwat, A., Yubonchit, S., Bui Van, D., 2022. Rainfall threshold for landslide warning in the southern Thailand – an integrated landslide susceptibility map with rainfall event – duration Threshold. Journal of Ecological Engineering 23 (12), 124–133.

Samodra, G., Ramadhan, M.F., Sartohadi, J., Setiawan, M.A., Christanto, N., Sukmawijaya, A., 2020. Characterization of displacement and internal structure of landslides from multitemporal UAV and ERT imaging. Landslides 17 (10), 2455–2468.

Sheehan, R.J., Doll, W.E., Mandell, W.A., 2005. An evaluation of methods and available software for seismic refraction tomography analysis. JEEG 10, 21–34.

Solberg, I.L., Long, M., Baranwal, V.C., Gylland, A.S., Rønning, J.S., 2016. Geophysical and geotechnical studies of geology and sediment properties at a quick-clay landslide site at Esp, Trondheim, Norway. Eng. Geol. 208, 214–230.

Thakur, M., Kumar, N., Dhiman, R.K., Malik, J.N., 2023. Geological and geotechnical investigations of the Sataun landslide along the Active Sirmauri Tal Fault, Sataun, Northwestern Himalaya. India. Landslides 20 (5), 1045–1063.

Whiteley, J.S., Chambers, J.E., Uhlemann, S., Wilkinson, P.B., Kendall, J.M., 2019. Geophysical monitoring of moisture-induced landslides: a review. Rev. Geophys. 57.
Yilmaz, S., 2007. Investigation of gürbulak landslide Using 2D electrical resistivity image profiling method (Trabzon, Northeastern Turkey). J. Environ. Eng. Geophys. 12 (2), 199–205.
Zakaria, M.T., Mohd Muztaza, N., Zabidi, H., Salleh, A.N., Mahmud, N., Samsudin, N., Rosli, F.N., Olugbenga, A.T., Jia, T.Y., 2021. 2-D Cross-plot model analysis using integrated geophysical methods for landslides assessment. Appl. Sci. 11 (2), 747.